Hindawi
Advances in Materials Science and Engineering
Volume 2019, Article ID 2842416, 11 pages
https://doi.org/10.1155/2019/2842416

Research Article

Three-Point Bending Fatigue Test of TiAl6V4 Titanium Alloy at Room Temperature

Juraj Belan, Lenka Kuchariková, Eva Tillová, and Mária Chalupová

Department of Materials Engineering, Faculty of Mechanical Engineering, University of Žilina, Univerzitná 8215/1, 01026 Žilina, Slovakia

Correspondence should be addressed to Juraj Belan; juraj.belan@fstroj.uniza.sk

Received 28 June 2019; Accepted 21 August 2019; Published 10 September 2019

Guest Editor: Dariusz Rozumek

A polycrystalline alpha-beta TiAl6V4 alloy in the annealed condition was used for the three-point bending fatigue test at frequency f~100 Hz. The static preload $F_{stat.} = -15$ kN and variable dynamic force $F_{dyn.} = -7$ kN to -13.5 kN were set as fatigue test loading parameters. The fatigue life S-N curve presented the stress amplitude σ_a as a function of a number of cycles to fracture N_f. A limiting number of cycles to run out of 2.0×10^7 cycles were chosen for the 3-point fatigue tests of rectangular specimens. In addition, the Smith diagram was used to predict the fatigue life. The alpha lamellae width has a significant influence on fatigue life. It is assumed that the increasing width of alpha lamellae decreases fatigue life. A comparison of fatigue results with given alpha lamellae width in our material to the results of other researchers was performed. The SEM fractography was performed with an accent to reveal the initiation sites of crack at low and high load stresses and mechanism of crack propagation for the fatigue part of fracture.

1. Introduction

The TiAl6V4 alloy has a relatively high resistance in cyclic loading [1–4]. However, the course of fatigue damage, however, depends on the content of the additive elements, microstructure, surface treatment, and size and type of applied stresses. The fatigue strength value for smooth samples is more than 50% of the tensile strength, but it is largely dependent on surface quality. The greater the roughness of the surface, or the surface saturated with oxygen or nitrogen, the worse the fatigue properties of titanium. The presence of a notch causes a fatigue reduction of 30–35%. The fatigue range for titanium alloys is reached at 10^6-10^7 cycles, but it is dependent on the load frequency [5].

Generally, the grain size of materials is a very important characteristic of fatigue life. Leyens and Peters in their work [2] present results that the reduction of grain size from 110 to 6 μm for commercially pure titanium increases the fatigue strength from 160 to 210 MPa. Likewise, the fatigue strength increases after increasing strength via work hardening. In addition, Gao et al. [6] and Moussaoui et al. [7] have performed an intensive study about influence α grain size, degree of age hardening, and oxygen content on fatigue life of TiAl6V4. They show that the fatigue properties of two-phase near $-\alpha$ and $\alpha + \beta$ alloys are strongly influenced by the morphology and arrangements of the two phases α and β (β grain size, colony size of α and β lamellae, and the width of α lamellae in lamellar microstructures). Another research was performed by Peters et al. and Wagner et al. [8, 9] report that reducing off the α lamellae width from 10 to 0.50 μm in lamellar microstructures raises the fatigue strength from 480 to 675 MPa.

They also show that reducing the grain size from 12 to 2 μm in equiaxed microstructures increases fatigue strength from 560 to 720 MPa [8]. For duplex structures, reducing the α lamellae width in a lamellar matrix from 1 to 0.5 μm leads to an increase in fatigue strength from 480 to 575 MPa [9].

For the fatigue process as itself, it is a well-known fact that most of the fatigue cracks initiate at free surface (due to surface roughness, oxide presence, or carbide particles). The fatigue process may also start from so-called "fish-eye," what is a typical structural phenomenon when fatigue crack

initiates close to free surface on inclusions (oxide or carbide particles). This phenomenon occurs only in special cases when a very high-cycle fatigue test (over 10^9 cycles to failure) is performed at low-stress amplitude. Zuo et al. [10] have confirmed this phenomenon on this type of alloy with bimodal and basket-weave microstructure. This kind of initiation was not confirmed at low-cycle or high-cycle fatigue of TiAl6V4 alloy. Wagner and Lütjering discussed three various fatigue crack initiation sites in their work [11]. They have shown that fatigue crack initiation sites are related to microstructure. The first type of the fatigue crack initiation site is for lamellar microstructure where fatigue cracks initiate at slip bands of the α lamellae as itself or at connection areas between α lamellae and primary β grain boundaries. The α lamellae width has significant effect on slowing down dislocation movement which is closely related to fatigue crack initiation, and on the contrary, it has influence on fatigue strength and yield stress too. The second type of the fatigue crack initiation site is for equiaxed structures. The fatigue cracks initiate in concert with slip bands inside α grains at these types of microstructures. Therefore, fatigue strength is affected by the grain size and on grain size is yield stress dependent as well. The third type of the fatigue crack initiation site is for duplex structures. The fatigue cracks may initiate in the lamellar matrix (interface the lamellar matrix/the primary α phase), or in the primary α phase as itself. Kuhlman [12] showed that the fatigue crack initiation site also depends on the cooling rate. Boyer and Puschnik et al. [13, 14] in their works have discussed the effect of the volume fraction and size of the primary α phase on fatigue crack initiation sites.

The influence of microstructure on fatigue properties of Ti6Al4V alloys at high-cycle fatigue is discussed in the works of Wu et al. [15] and Crupi et al. [16]. Their results prove the fact that various microstructures decrease (from bimodal, lamellar to equiaxed) high-cycle fatigue strength. About Ti6Al4V bimodal structures, the high-cycle fatigue strength is strongly affected by the primary α phase volume and grain size. In the initial stage, the high-cycle fatigue strength increases. However, it gradually decreases with increasing amount and size of the primary alpha phase. A similar effect of decreasing high-cycle fatigue strength can also be observed in the case of equiaxed or lamellar microstructures of Ti6Al4V alloy. Essentially, it can be generalized that the fatigue strength of the Ti6Al4V alloy decreases, either due to the increase in the alpha-phase grain or by increasing the width of the alpha-phase lamellae.

Another factor affecting the fatigue strength of the Ti6Al4V alloy is the load frequency. This issue was studied by Furuya and Takeuchi [17]. Based on their work, it is possible to state that the results of fatigue tests at ultrasonic frequency are similar, respectively, comparable to results performed at 100 Hz load frequency. However, this is only true if the fatigue crack has initiated below the alloy surface. In the case of the Ti6Al4V alloy, when the fatigue crack initiated on the surface, it was shown that the fatigue strength was higher in the tests performed at the ultrasonic frequency than in the conventional 100 Hz frequency. The mean stress effect on fatigue strength is commonly evaluated by a modified Goodman's or Smith diagram. For the Ti6Al4V alloy, according to modified Goodman's (or Smith) diagram, the fatigue strength is considered safe when reaching 10^7 at conventional load frequencies.

Morrissey and Nicholas [18] also studied the impact of load frequency on strain rate or temperature increase due to internal damping. They compare data from ultrasonic tests, servohydraulic test systems (~60 Hz), and electromagnetic shaker systems (400 Hz). According to their data comparison, there are no frequency effects. The comparison of S-N results at ultrasonic and conventional frequencies is shown in Figure 1.

The aim of this paper is to provide information about fatigue resistance of the TiAl6V4 alloy in the annealed condition at the three-point bending loading test at frequency f~100.0 Hz [19, 20] with the run-out number of cycles N_f in range 10^6 to 2.0×10^7 and to compare it with results in references [8, 9, 15] to show how the bending load and microstructure (α lamellae length and width or primary α (α_p) grain size) affect the fatigue life. There is an assumption that bending load should decrease fatigue life of alloy due to more complex stress course in the specimen. The fatigue test frequency influence or sample heating due to internal damping at 100 Hz is not expected according to references [17, 18].

2. Materials and Methods

The $\alpha + \beta$ mixed TiAl6V4 (GRADE 5) titanium alloy was used as experimental material. The alloy chemical composition and selected mechanical properties according to the certificate of quality and weight (the alloy was supplied by BIBUS Metals AG, CZ, with heat No. HX-032) are given in Table 1. The alloy was in the annealed condition. Boyer had described in his work [13, 21] four common heat-treatments for $\alpha + \beta$ alloys, namely, Ti6Al4V. According to its work, the most suitable treatment for increasing the fatigue properties and achieving the reasonable fatigue crack growth is mill annealing (MA or A). After this treatment, the strength of about 896 MPa and moderate fracture toughness 66 MPa·m^{-2} are achieved. The microstructure of experimental material is shown in Figure 2. It consists of α-phase lamellae which is considered as the hexagonal close-packed phase (HCP) presented at lower temperatures (up to 886°C) situated in β grains (body centred cubic, BCC, for temperatures from 886°C to melting temperature 1660°C) (Figure 2(a)). The arrangement of α-phase lamellae is presented more in detail in Figure 2(b), and as is obvious, it creates the "envelop" of aluminium solid solution in the base titanium matrix.

Samples for the three-point bending test were supplied by BIBUS METALS AG. Samples were cut to $11 \times 10 \times 50$ mm blocks. The specimen surface was sanded using a LaboPol-25 double-disk grinder, where the sample was ground on the grinding disk with a grain size of 400 (grinding in direction 1) and 600 (grinding in a direction perpendicular to direction 1) at 250 rpm. The sample was next rinsed in warm water and alcohol and dried after each step.

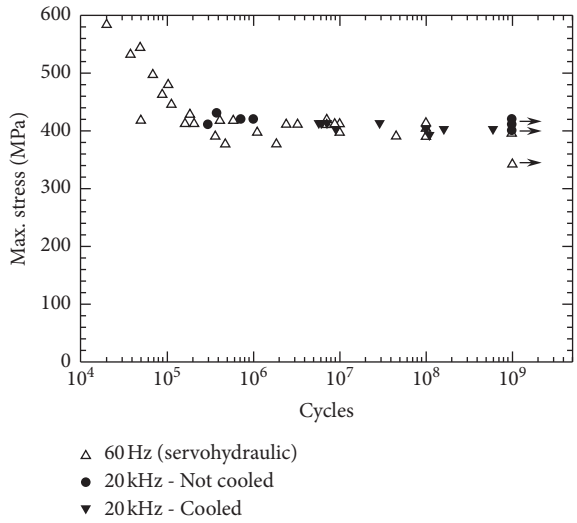

Figure 1: Comparison of S-N results at ultrasonic and conventional frequencies [18].

Two single-disk MTH polishers were used for polishing. In the first step, diamond paste D2 with a diamond grain size of 2 μm was added to the sample using a Mol roll at 300 rpm. The disk was moistened with alcohol during polishing, and the sample was polished against the counterclockwise rotation of the disc. In the second step, the D07 paste with a diamond grain size of 0.7 μm was applied using a Nap spin at 300 rpm. The disk was moistened with alcohol during polishing, and the sample was polished against the counterclockwise rotation of the disc. The sample was rinsed in warm water and alcohol and dried after each step. One side of the specimen was over polished due to the good observation of fatigue crack propagation. The surface roughness was measured by the MITUTOYO-ABSOLUTE-DIGIMATIC-HEIGHTGAGE device to compare how the surface roughness affects the fatigue life.

The fatigue test at the three-point bending was performed on a ZWICK/ROELL Amsler 150HFP 5100 resonance pulsator (Figure 3(a)) on 10 experimental specimens at room temperature 22°C ± 5.0°C. The specimens were numbered from 1 to 10. Vibrophore Amsler 150HFP 5100 is for fatigue testing of materials or components by applying sinusoid loads using the resonance principle (testing frequency range 35–300 Hz) with constant or variable amplitude (maximum force amplitude range is ±75 kN) and mean load (maximum mean load is ±150 kN). It provides fatigue testing of materials and components, e.g., fatigue tests according to DIN 50100 (S-N curve) for tensile stress and compressive and alternating stress ranges. Testing can be performed either force controlled (precision force measurement through calibration according to DIN 51 221 and US MIL Std. 1312 B) or strain controlled (two measurement channels for additional extensometers—force and strain; optional extensible through two measuring inputs). Tests can also be carried out under various environmental conditions, e.g., temperature range from cryogenic temperatures in a liquid nitrogen atmosphere to high-temperature testing up to 1200°C (for pushpull loading only). In addition, torsion and bending tests can also be carried out. The parameters of the test were set as follows: the static preload force $F_{\text{stat.}} = -15.0$ kN; the dynamic load was represented by dynamic force varied $F_{\text{dyn.}} = -7.00$ kN to -13.5 kN; frequency during the test was $f = 82.50$ Hz–108.6 Hz; stress cycle asymmetry $R < 1$; the number of cycles was set on value 2.0×10^7 representing the run-out. For titanium alloys, this value is considered as the fatigue limit (if the specimens withstand the 2.0×10^7 cycles at set stress amplitude without break, then the fatigue limit is reached).

The sample (of the size 10 mm × 11 mm × 50 mm) was positioned as shown in Figure 3(b), and it means that the center of the sample was loaded by the main force. To prevent specimens heating during the fatigue test, the specimens were cooled by an external fan. The stress amplitude σ_a is calculated according to the following equation:

$$\sigma_a = \frac{3 \times F \times L}{2 \times b \times h^2} \text{ (MPa)}. \quad (1)$$

where F is the applied dynamic force [N], L is the distance of supports which is 30 mm, b is the sample width which is 10 mm, h is the sample height which is 11 mm, and σ_a is the maximum amplitude (MPa). The S-N curve was drawn. The Smith diagram discusses the relation between mean stress σ_m and stress amplitude σ_a and provides information about the secure area of loading at various values of mean stress σ_m.

The three-point bending loading is not so common way to obtain fatigue life values in comparison to push-pull loading with a coefficient of asymmetry $R = -1$. Three-point bending fatigue loading provides more complex loading of specimens due to the shifting of mean stress to negative values with a coefficient of asymmetry $R < 1$. It means that the specimen is preloaded by negative static force with a higher value than the stress amplitude which results in more complex loading in the center of the specimen. There is an expectation that fatigue life shifts to lower values due to more complex loading compared to push-pull results.

Metallography specimens were prepared by cutting with MTH Micron 3000 precise saw and then mounting into bakelite mixture in Struers CitoPress 1 and finally ground and polished using Struers TegraSystem (TegraPol-15 and TegraForce-1) and a special program for titanium alloys. Grinding and polishing consist of a few steps: grinding with SiC sandpaper No. 320, followed by fine grinding with Largo grinding disk and emulsion Allegro Largo with 9 μm grains. The first step of polishing is performed with Dac polishing disk with an emulsion of Diap 3 μm grains and fine polishing with OP-S lubricant with 0.25 μm grains. The sample was rinsed in warm water and alcohol and dried after each step. This procedure was applied on specimens for light microscopy (LM) and for scanning electron microscopy (SEM) analysis as well.

After polishing, the sample was etched; the specimen surface was immersed into 10% solution of HF for 7 seconds and then rinsed with warm water and alcohol and dried by hot air. The microstructure was observed on light microscope

Table 1: Chemical composition in wt.% and selected mechanical properties of the TiAl6V4 alloy.

Chemical composition (wt.%)								
	Fe	C	N	H	O	Al	V	Ti
Specification condition	≤0.40	≤0.08	≤0.05	≤0.015	≤0.20	5.50–6.75	3.50–4.50	Reminder
Analyses	0.059	0.012	0.004	0.001	0.097	6.04	4.00	89.8
Mechanical properties								
	Ultimate tensile strength UTS (MPa)		Yield strength 0.2% (MPa)		Elongation (%)		Hardness HV	
Specification condition	Min. 895		Min. 828		Min. 10			
Longitudinal	1011		951		15		266	
Transverse	1023		971		14			

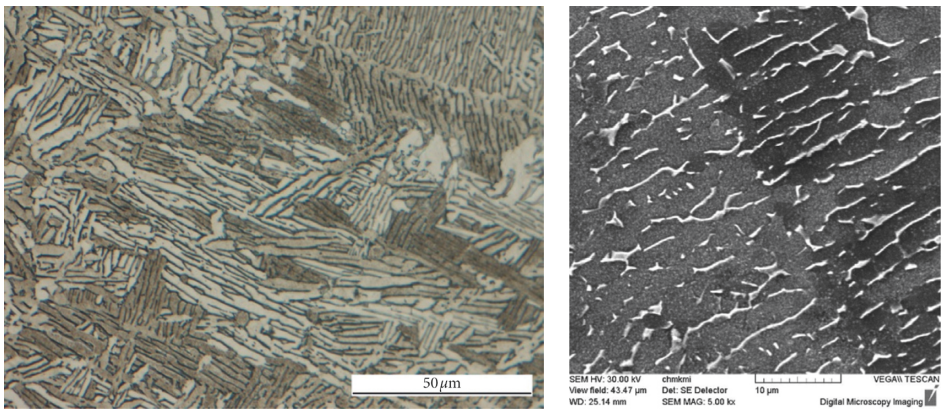

(a) (b)

Figure 2: The micrographs of TiAl6V4 alloy: (a) light microscopy, 10% HF acid etching, and (b) SEM observation, equiaxed microstructure with β grains, and α-phase lamellae.

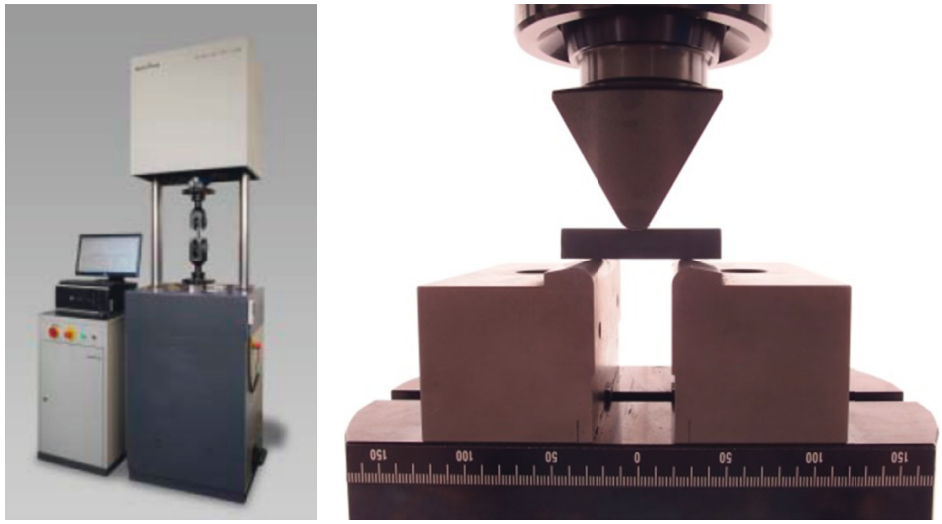

(a) (b)

Figure 3: Three-point bending fatigue test: (a) ZWICK/ROELL Amsler 150HFP 5100 resonance pulsator and (b) sample position on pulsator at the three-point bending fatigue test.

Neophot 32. The grain size and α lamellae length and width were measured by using NIS-elements 4.20 metallography software.

The fractography analysis of specimens' surface after the fatigue test was performed using the TESCAN VEGA LMU II scanning electron microscope with the aim to detect the

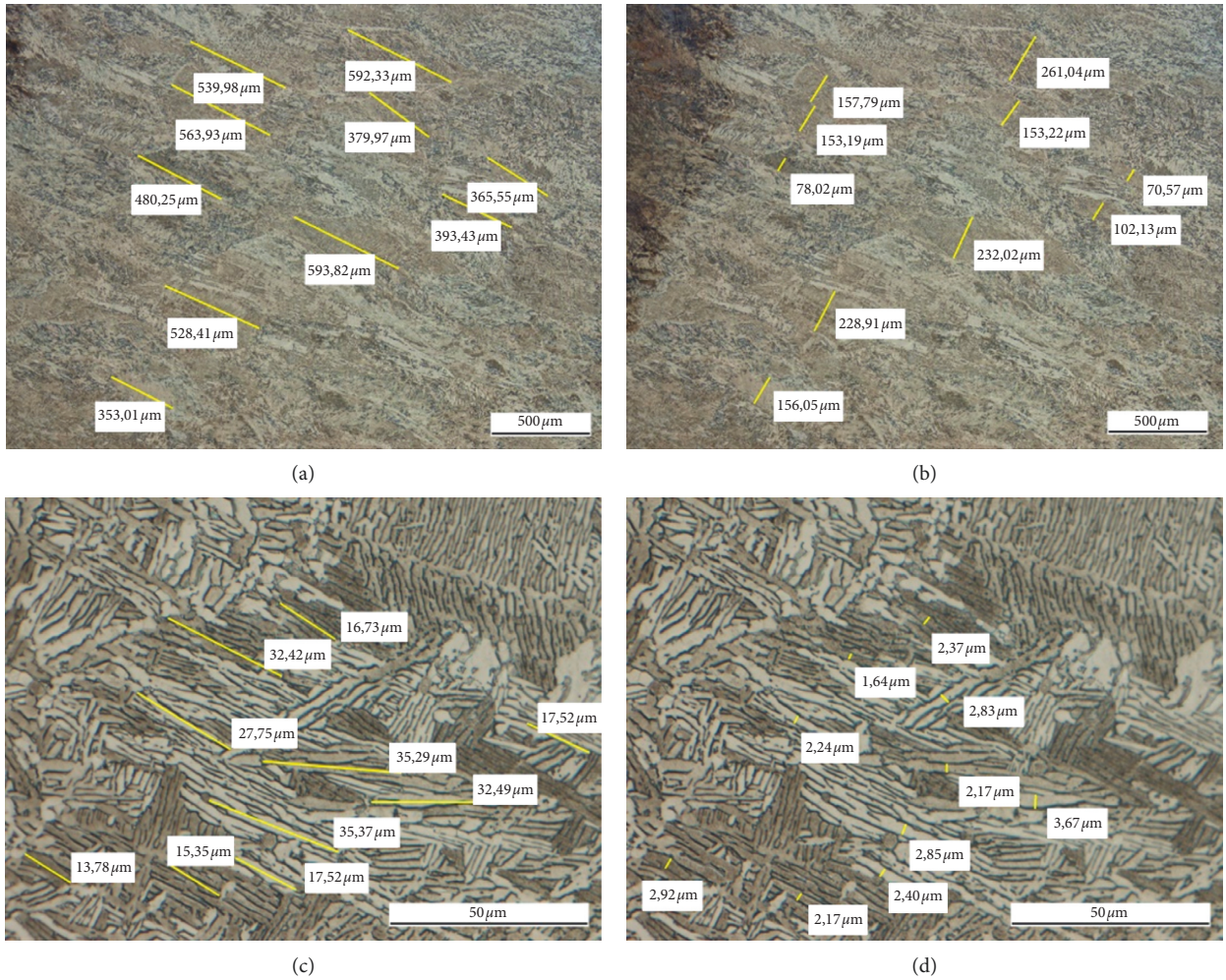

Figure 4: The microstructure of experimental material—TiAl6V4 alloy: (a) the grain length measurement, (b) the width of grains measurements, and (c, d) α—lamellae measurements, 10% HF acid etching.

fatigue initiation site, fatigue crack propagation, and static fracture area analysis.

3. Results and Discussion

3.1. Microstructure. The microstructure of experimental material is documented in Figures 2 and 4. It consists of elongated grains of α lamellae in the transformed β phase (Figure 3). The average length of the grains is 479.1 μm (Figure 4(a)), and the average width is 159.3 μm (Figure 4(b)). The average length of the α lamellae is 24.42 μm (Figure 4(c)), and the average thickness is 2.530 μm (Figure 4(d)). This microstructure is in good agreement with β heat-treated TiAl6V4 alloy at 1020°C/20 min/FC with Widmanstätten α structure presented on prior β grain boundaries reported in Videhi Arun work [22]. The morphology of the Widmanstätten α phase may change from a colony of similarly aligned α lath to a basket-weave arrangement with an increase in the cooling rate or alloying content. From the present knowledge, the dependence of the fatigue life on the lamellar α phase is known. The larger the lamella dimensions are, the lower the fatigue life of the alloy is. To confirm this phenomenon, it would be advisable to perform tests for a more fine-grained structure and to compare the obtained values.

3.2. Fatigue Test Results. The S-N curve is shown in Figure 5. The experimental data were interpolated and the following coefficients of the Basquin [23, 24] equation were obtained:

$$\sigma_a = 912.92 \times N_f^{-0.044} \text{ (MPa)}. \quad (2)$$

From the S-N curve of the fatigue life for σ_a, it is clear that, after the translation of the resulting values of the number of cycles N_f to the failure and the stress amplitude σ_a by the power regression curve, the scattering of the obtained values is relatively small. Therefore, the maximum stress amplitude σ_a in tested material at a given number of N_f cycles can be predicted fairly accurately from equation (2).

The fatigue stress σ_c (defined as the highest stress at which the test bar = specimen is not broken even after the set number of cycles 2.0×10^7 has been exceeded) was calculated according to equation (1) as the medium value from three run-out stress amplitudes, and its value is 431 MPa. The

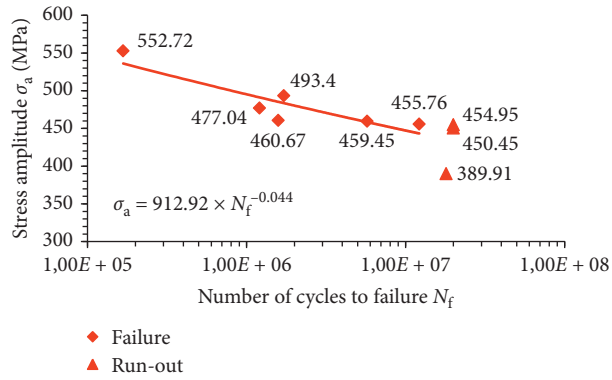

Figure 5: S-N curve for TiAl6V4 alloy at three-point bending fatigue loading at room temperature.

Table 2: Fatigue test results with used specimen numbering.

Spec. no.	Number of cycles N_f	Mean stress σ_m (MPa)	Stress amplitude σ_a (MPa)	Maximum bending stress σ_O (MPa)	Notice
1	2.0×10^7	613.0	287.0	901.0	Polished, run-out
2	1.8×10^7		389.0	1003.0	Polished, break
3	1.7×10^6		493.0	1107.0	Polished, break
4	1.6×10^5		552.0	1166.0	Polished, break
5	2.0×10^7		450.0	1064.0	Polished, run-out
6	1.2×10^6		477.0	1090.0	Polished, break
7	1.6×10^6		460.0	1074.0	Polished, break
8	2.0×10^7		454.0	1068.0	Polished, run-out
9	5.7×10^6		459.0	1073.0	Polished, break
10	1.2×10^7		455.0	1069.0	Polished, break
11	5.3×10^4		455.0	1068.0	Non-polished, not included in S-N curve
12	6.4×10^4		459.0	1073.0	Non-polished, not included in S-N curve

results for all specimens used at the fatigue test with specimen numbering are shown in Table 2.

Results obtained after the three-point bending fatigue test with load cycle asymmetry $R < 1$ were compared to results of Peters et al. and Wagner et al. [8, 9], Wu et al. [15], and Morrissey and Nicholas [18]. They have used common push-pull loading at $R = -1$. The results comparison shows a difference about 30.0 MPa–40.0 MPa lower in fatigue life and stress amplitude at run-out. This result shows a more complex character of fatigue specimens loading than simple push-pull loading.

The three-point bending loading includes a compression loading and a tension loading as well, and the specimen is subjected not only to direct stress but to bending moment with increasing value when approaching the specimen centre.

The influence of the mean stress σ_m on the fatigue stress σ_c is expressed by the Smith diagram [17, 25] in Figure 6. The region bounded by red indicates the area of the stress, where there is no break even after the theoretically unlimited number of cycles at the given mean stress σ_m and the amplitude of the stress σ_a cycles. The diagram is designed for the compressive stress area, and therefore, it is advantageous for its construction to use the values of the yield bearing strength and ultimate bearing strength [26] that involve a more complex load. It can be seen from the diagram that the fatigue resistance of the TiAl6V4 alloy increases with the decreasing amplitude of the stress σ_a.

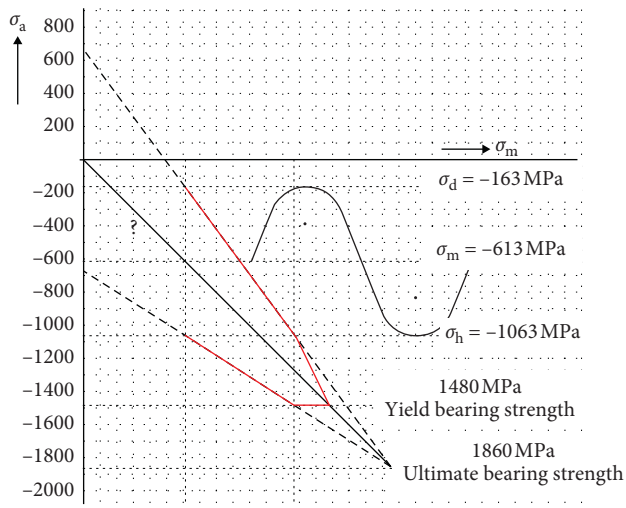

Figure 6: Smith fatigue life diagram [25] for the TiAl6V4 alloy.

Based on TiAl6V4 titanium alloy analyses with grains with an average length of 479 μm and a width of 159 μm, and

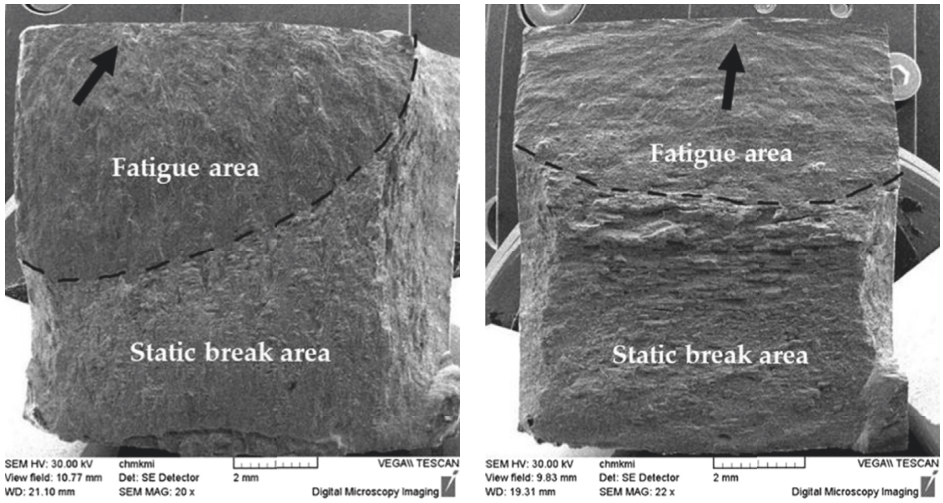

(a) (b)

FIGURE 7: Overall view on fracture surface, initiation sites are marked by arrows: (a) spec. no. 9, $F_{dyn} = -11$ kN; $\sigma_{Omax} = 1073$ MPa; $\sigma_a = 459$ MPa and (b) spec. no. 3, $F_{dyn} = -12$ kN; $\sigma_{Omax} = 1107$ MPa; $\sigma_a = 493$ MPa, SEM.

α lamellae with an average length of 24.4 μm and a width of 2.53 μm, it can be concluded that the fatigue interval σ_c is strongly dependent on the stress amplitude σ_a. According to the established rules obtained from numerous experiments [23, 24], the fatigue limit σ_c at the load push-pull and $R = -1$ corresponds to approximately 50% of ultimate tensile stress. Based on the constructed Smith diagram, it can be assumed that, for $\sigma_m = 0$ MPa, σ_c~650 MPa and UTS~1300 MPa, which corresponds to our calculated value UTS = 1323 MPa.

3.3. SEM Fractography. Figure 7 shows the fracture surface where the fatigue region, static break area, and a fatigue crack initiation site are marked (black arrow). The diminution of the fatigue region (Figure 7(b)) with the increasing value of the dynamic loading force and the stress amplitude σ_a as well is visible when macro-fractographic images are compared.

In Figure 8, the images of samples No. 9 and 7 of the fatigue crack initiation region are shown (Figures 8(a) and 8(b)). The fatigue crack in both cases initiated at the free surface of the polished samples at the sites of the highest concentration of stress. Major crack propagation proceeded from the free surface by transcrystalline cleavage of TiAl6V4 alloy grains with the cleavage facets observed at the crack initiation site. The cleavage facets of samples 9 and 7 are shown in Figures 8(c) and 8(d).

Micro-fractographic images of cleavage facets created by transcrystalline cleavage of TiAl6V4 alloy grains along the direction of propagation of the magistral fatigue crack are notable in Figure 9. In Figure 9(a), the transcrystalline cleavage facet with river morphology is visible. The river reliefs on facets are created due to plastic deformation that preceded the crack formation and its growth, presence of grain boundaries, or α-phase lamellae. The origin of the rivers also means energy consumption, which slows down the rate of propagation of the fatigue crack tip. In another case, especially at higher stress amplitude, the transcrystalline cleavage failure of β grains with a higher degree of cleavage has occurred (Figure 9(b)).

In the area of the stable fatigue crack propagation, the striations (Figure 10(a)) are visible on the surface, indicating the position of the crack tip at the given moment and creating ridges spreading from the initiation site. These ridges are perpendicular to the direction of magistral fatigue crack propagation. Another characteristic feature of the fatigue process is the secondary crack parallel to the advancing fatigue crack front documented in Figure 10(b).

From the comparison of the individual micrographs, it is clear that the amount of secondary cracks increases with the rising value of the stress amplitude. The change in the direction of the striation propagation due to the change in the direction of the magistral fatigue crack growth is shown in Figure 11(a). The area of static failure documented in Figure 11(b) is characterized by a transcrystalline ductile fracture with dimple morphology. A ductile fracture occurs by coalescence of microcells that nucleate at the grain boundaries, secondary-phase particles, or inclusions. The orientation of the holes varies with the orientation of the applied stress and β grain orientation to the applied load as well.

The fractography analysis revealed that the polished surface of samples had a single initiation site just below the surface of the sample where the characteristic of initiation and propagation of the fatigue crack was the transcrystalline cleavage of TiAl6V4 alloy β grains, which is supported by images of transcrystalline cleavage facets in the fatigue crack initiation region. The smaller the area of fatigue fracture was, the higher the amplitude of the stress σ_a was. Striations and secondary fatigue cracks, which are features of fatigue fracture, have also been observed in this area. The transcrystalline cleavage failure was caused by loss of coherency at the α lamella interface and the transformed β grain matrix.

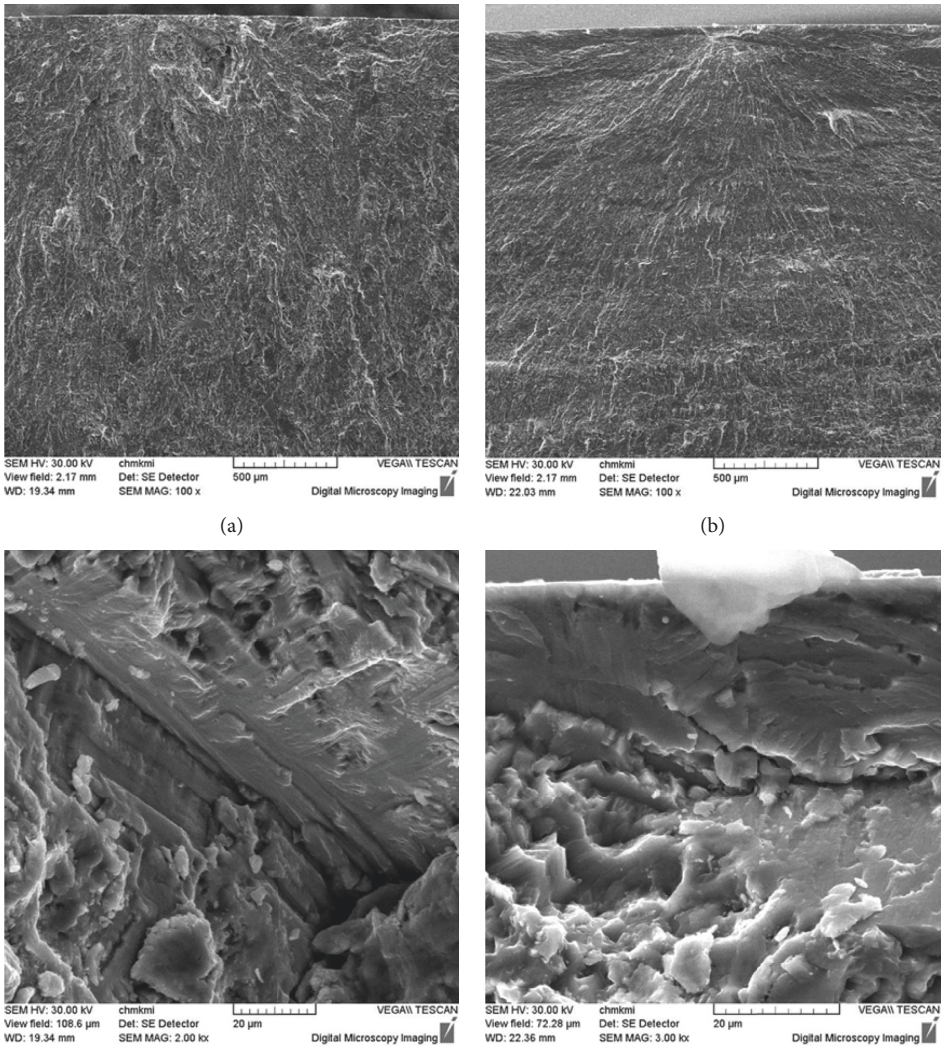

Figure 8: Initiation sites of fatigue crack on the free surface: (a) spec. no. 9, (b) spec. no. 7. Cleavage facets made by transcrystalline cleavage failure of the TiAl6V4 alloy grain at the fatigue crack initiation sites: (c) spec. no. 9; (d) spec. no. 7, details of the initiation site, SEM.

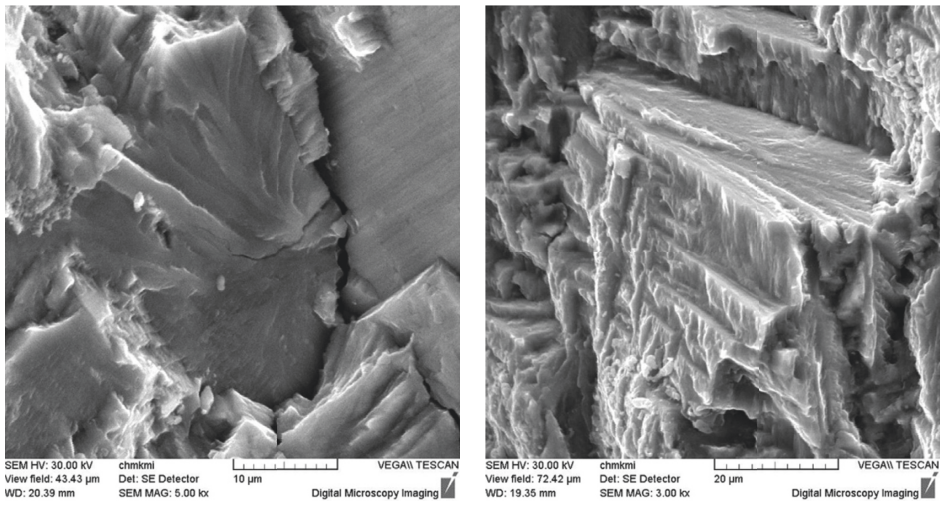

Figure 9: Details of transcrystalline cleavage failure of TiAl6V4 grains: (a) transcrystalline cleavage facet with river morphology; (b) transcrystalline cleavage failure of grains with a higher degree of cleavage, SEM.

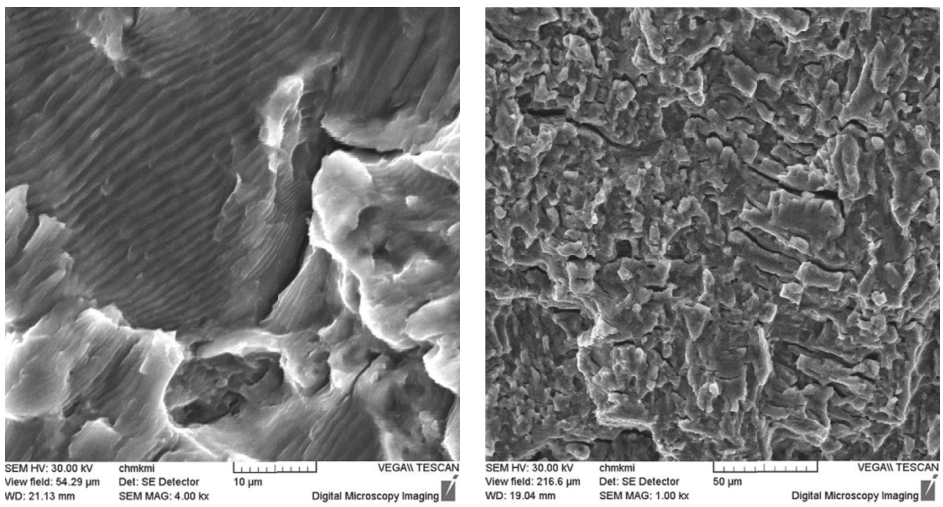

(a) (b)

Figure 10: Striation (a) in a perpendicular direction to fatigue crack propagation and secondary fatigue cracks (b) parallel to the advancing crack front, SEM.

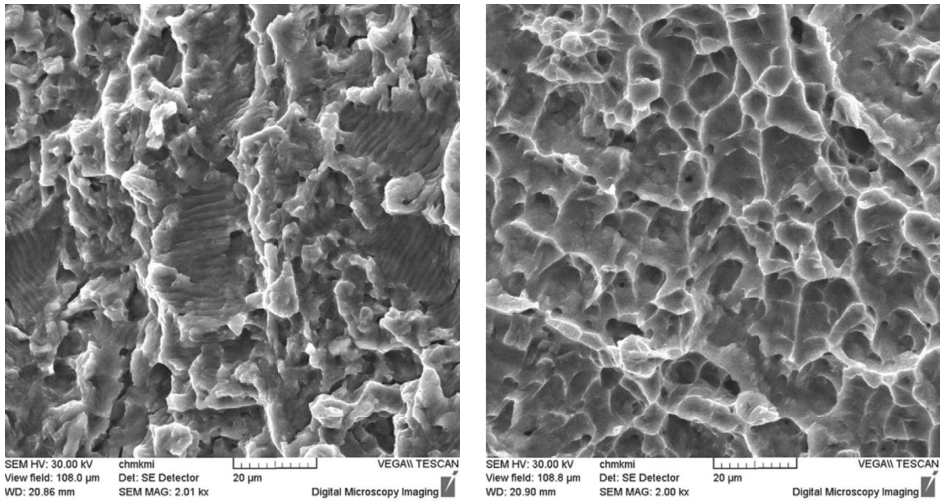

(a) (b)

Figure 11: Change in the direction of striation propagation (a) and static transcrystalline ductile fracture with dimple morphology (b), SEM.

3.4. Influence of Surface Roughness on Fatigue Life and Hardness Measurements. The surface quality has a significant influence on the fatigue life of the α-β TiAl6V4 alloy. In the fatigue test, all specimens (except of two which of course were not included in S-N curve results) were polished. Polished specimens have surface roughness $R_a = 0.252$–$0.265\,\mu$m. Specimen No. 8 at loading $\sigma_{Omax} = 1068$ MPa withstands the 2.0×10^7 cycles (it was run out, specimen without breaking). Specimen No. 9 at $\sigma_{Omax} = 1073$ MPa withstands the 5.75×10^6 cycles (specimen with break). For nonpolished specimens with a surface roughness $R_a = 3.95$–$5.12\,\mu$m, the number of cycles to failure has dramatically decreased. For specimen No. 11, it was 5.32×10^4 cycles at the same stress level as specimen No. 8, and for specimen No. 12, it was 6.39×10^4 cycles at the same stress level as specimen No. 9. The fatigue life or the number of cycles to failure was decreased by about 74% for specimen No. 11 and about 97% for specimen No. 12.

The maximum bending stress $\sigma_{Omax} = 1090$ MPa which is obviously higher then ultimate tensile stress UTS = 1011 MPa (in the longitudinal direction) reported for this material in the material list was applied at the fatigue test. To explain this phenomenon, the hardness measurements of material were performed and the results of measurement are shown in Table 3. The values are the mean values of four hardness measurements.

There is a relation between the hardness and the material toughness, and it is expressed by using equation (3), where k is the coefficient that depends on the material type, and for titanium alloys, $k = 3$-4. The volumes of the k coefficient for

Table 3: TiAl6V4 hardness measurement.

	Material list hardness 266 HV		
Average value	VICKERS	BRINELL	ROCKWELL
	346 HV 10/6	299 HBW 5/750	32 HRC

various material types and their effect on final UTS were discussed more in detail in the work of Tabor et al. [27] and Zhang et al. [28]:

$$\text{UTS} = k \times \text{HV (MPa)}. \quad (3)$$

For our experimental material TiAl6V4 alloy, $k = 3.85$ based on calculation from values provided by the supplier. According to this, the calculated ultimate tensile stress UTS = 1323 MPa. This value is over 301 MPa higher than that reported in the material list. This difference in material toughness and hardness is possible due to secondary hardening, which was not reported in the material list.

4. Conclusions

The titanium alloy TiAl6V4 was subjected to three-point bending fatigue loading at a frequency ~100 Hz for a high number of cycles 2.0×10^7 at room temperature 22°C ± 5.0°C. It was shown that fatigue crack initiates from free surface and has single initiation at lower amplitudes of stress σ_a and multiple initiation sites when higher stress amplitude σ_a was used.

The fatigue life was reached after a 2.0×10^7 number of cycles, and it was set on $\sigma_c = 431$ MPa. This value is about 30 MPa–40 MPa lower compared to common push-pull fatigue results on this alloy with similar equiaxed microstructure and α lamellae width as reported in experiments of other authors. However, it is necessary to take into count the different loading modes, specimen shape, and surface finishing of samples used at push-pull loading. The comparison with push-pull loading is performed due to the lack of data about the three-point bending fatigue test for this alloy in English.

The results show that a three-point bend is more complex loading and is more suitable for obtaining a fatigue life for advanced materials compared to the commonly used push-pull loads. The three-point bending loading includes both compression loading and tension loading, and a specimen is not subjected to direct stress only for the whole cross section but to the bending moment with increasing value when approaching the specimen center.

Data Availability

The data used to support the findings of this study are available from the corresponding author upon request. The data used for Figure 1 and equation (3) are available in [18] and [27, 28], respectively.

Conflicts of Interest

The authors declare that they have no conflicts of interest.

Acknowledgments

The project presented in this article was supported by Scientific Grant Agency of Ministry of Education of the Slovak Republic (nos. 012ŽU-4/2019 and 049ŽU-4/2017) and project EU ITMS 26220220154.

References

[1] M. J. Donachie, *Titanium: A Technical Guide*, ASM International: Materials Park, Cleveland, OH, USA, 2nd edition, 2000.

[2] C. H. Leyens and M. Peters, *Titanium and Titanium Alloys. Fundamentals and Applications*, WILEY-VCH Verlag GmbH & Co. KGaA, Weinheim, Germany, 2003.

[3] Y. Fan, W. Tian, Y. Guo, Z. Sun, and J. Xu, "Relationships among the microstructure, mechanical properties, and fatigue behavior in thin Ti6Al4V," *Advances in Materials Science and Engineering*, vol. 2016, Article ID 7278267, 9 pages, 2016.

[4] K. S. Ravichandran and S. K. Jha, "High-cycle fatigue resistance in beta/titanium alloys," *JOM*, vol. 53, no. 3, pp. 30–35, 2000.

[5] C. Bathias and A. Pineau, "Fatigue of materials and structures," in *Fatigue of Materials and Structures*, C. Bathias and A. Pineau, Eds., , ISTE Ltd., London, UK, 1st edition, 2010.

[6] H.-J. Gao, Y.-D. Zhang, Q. Wu, and J. Song, "Experimental investigation on the fatigue life of Ti-6Al-4V treated by vibratory stress relief," *Metals*, vol. 7, no. 5, p. 158, 2017.

[7] K. Moussaoui, M. Mousseigne, J. Senatore, R. Chieragatti, and P. Lamesle, "Influence of milling on the fatigue lifetime of a Ti6Al4V titanium alloy," *Metals*, vol. 5, no. 3, pp. 1148–1162, 2015.

[8] M. Peters, A. Gysler, and G. Lütjering, "Influence of texture on fatigue properties of Ti-6Al-4V," *Metallurgical and Materials Transactions A*, vol. 15, no. 8, pp. 1597–1605, 1984.

[9] L. Wagner, R. I. Jaffee, and G. Lütjering, "Influence of microstructure and texture on fatigue properties of Ti-6Al-4V," in *Microstructure/Property Relationships in Titanium Aluminides and Alloys*, R. R. Boyer, Ed., p. 521, TMSAIME, Pittsburgh, PA, USA, 1st edition, 1991.

[10] J. H. Zuo, Z. G. Wang, and E. H. Han, "Effect of microstructure on ultra-high cycle fatigue behaviour of Ti–6Al–4V," *Materials Science and Engineering: A*, vol. 473, no. 1-2, pp. 147–152, 2008.

[11] L. Wagner and G. Lütjering, "Microstructural influences on propagation of short cracks in an (Alpha + Beta) Ti-alloy," *Metallkde*, vol. 87, p. 369, 1987.

[12] G. W. Kuhlman, "A critical appraisal of thermomechanical processing of structural titanium alloys," in *Microstructure/Property Relationships in Titanium Aluminides and Alloys*, R. R. Boyer, Ed., p. 465, TMS-IME, Pittsburgh, PA, USA, 1st edition, 1991.

[13] R. R. Boyer and J. A. Hall, "Microstructure—property relationships in titanium alloys (critical review)," in *Proceedings of the Titanium World Conference, Titanium'92: Science and Technology, Symposium 7th World Titanium Congress*, F. H. Froes and I. Caplan, Eds., pp. 77–88, TMS.

[14] H. Puschnik, J. Fladischer, G. Lütjering, and R. I. Jaffee, "Optimization of service properties for titanium forgings with bimodal microstructure," in *Proceedings of the Titanium World Conference, Titanium'92: Science and Technology, Symposium 7th World Titanium Congress*, F. H. Froes and I. Caplan, Eds., pp. 131–140, TMS, San Diego, CA, USA, June 1993.

[15] G. Q. Wu, C. L. Shi, W. Sha, A. X. Sha, and H. R. Jiang, "Effect of microstructure on the fatigue properties of Ti-6Al-4V titanium alloys," *Materials & Design*, vol. 46, pp. 668–674, 2013.
[16] V. Crupi, G. Epasto, E. Guglielmino, and A. Squillace, "Influence of microstructure [alpha + beta and beta] on very high cycle fatigue behaviour of Ti-6Al-4V alloy," *International Journal of Fatigue*, vol. 95, pp. 64–75, 2017.
[17] Y. Furuya and E. Takeuchi, "Gigacycle fatigue properties of Ti-6Al-4V alloy under tensile mean stress," *Materials Science and Engineering: A*, vol. 598, pp. 135–140, 2014.
[18] R. J. Morrissey and T. Nicholas, "Fatigue strength of Ti–6Al–4V at very long lives," *International Journal of Fatigue*, vol. 27, no. 10–12, pp. 1608–1612, 2005.
[19] J. Belan, L. Kuchariková, A. Vaško, E. Tillová, and M. Chalupová, "Fatigue test of the inconel alloy 718 under three-point bending load at a low frequency," in *Advanced Structured Materials. Properties and Characterization of Modern Materials*, A. Öchsner and H. Altenbach, Eds., vol. 33pp. 261–270, Springer Science + Business Media Singapore Pre Ltd., Singapore, 1st edition, 2017.
[20] J. Belan, M. Jambor, L. Kuchariková, E. Tillová, M. Chalupová, and M. Matvija, "The SEM investigation of Inconel 718 fatigue process at various loading conditions," *Manufacturing Technology*, vol. 17, pp. 658–665, 2017.
[21] R. R. Boyer, "An overview on the use of titanium in the aerospace industry," *Materials Science and Engineering: A*, vol. 213, no. 1-2, pp. 103–114, 1996.
[22] J. Vydehi Arun, *Titanium Alloys: An Atlas of Structures and Fracture Features*, Taylor & Francis Group, Boca Raton, FL, USA, 1st edition, 2006.
[23] L. Trško, O. Bokůvka, F. Nový, and M. Guagliano, "Effect of severe shot peening on ultra-high-cycle fatigue of a low-alloy steel," *Materials & Design*, vol. 57, pp. 103–113, 2014.
[24] O. Bokůvka, G. Nicoletto, M. Guagliano et al., *Fatigue of Materials at Low and High-Frequency Loading*, University of Žilina, Žilina, Slovakia, 1st edition, 2014.
[25] J. Schijve, *Fatigue of Structures and Materials*, Springer, Amsterdam, Netherlands, 2nd edition, 2009.
[26] R. Boyer, G. Welsch, and E. W. Collings, *Materials Properties Handbook: Titanium Alloys*, ASM International, Materials Park, OH, USA, 1994.
[27] D. Tabor, "The Hardness of Metals," *Oxford Classic Texts in the Physical Sciences*p. 192, Oxford University Press, Oxford, UK, 1st edition, 2000.
[28] P. Zhang, S. X. Li, and Z. F. Zhang, "General relationship between strength and hardness," *Materials Science and Engineering: A*, vol. 529, pp. 62–73, 2011.